Environment International 190 (2024) 108820

Contents lists available at ScienceDirect

Environment International

journal homepage: www.elsevier.com/locate/envint

Full length article

Metabolic and phenotypic changes induced by PFAS exposure in two human hepatocyte cell models

Andi Alijagic [a,b,c,1], Lisanna Sinisalu [a,1], Daniel Duberg [a], Oleksandr Kotlyar [a,d], Nikolai Scherbak [a], Magnus Engwall [a], Matej Orešič [c,e,f], Tuulia Hyötyläinen [a,*]

[a] Man-Technology-Environment (MTM) Research Centre, School of Science and Technology, Örebro University, SE-701 82 Örebro, Sweden
[b] Inflammatory Response and Infection Susceptibility Centre (iRiSC), Faculty of Medicine and Health, Örebro University, Örebro SE-701 82, Sweden
[c] School of Medical Sciences, Faculty of Medicine and Health, Örebro University, SE-701 82 Örebro, Sweden
[d] Centre for Applied Autonomous Sensor Systems (AASS), Mobile Robotics and Olfaction Lab (MRO), Örebro University, SE-701 82 Örebro, Sweden
[e] Turku Centre for Biotechnology, University of Turku and Åbo Akademi University, FI-20520 Turku, Finland
[f] Department of Life Technologies, University of Turku, FI-20014 Turku, Finland

ARTICLE INFO

Keywords:
HepG2
HepaRG
PFAS
Lipidomics
Metabolomics
Bile acids
Cell Painting

ABSTRACT

PFAS are ubiquitous industrial chemicals with known adverse health effects, particularly on the liver. The liver, being a vital metabolic organ, is susceptible to PFAS-induced metabolic dysregulation, leading to conditions such as hepatotoxicity and metabolic disturbances. In this study, we investigated the phenotypic and metabolic responses of PFAS exposure using two hepatocyte models, HepG2 (male cell line) and HepaRG (female cell line), aiming to define phenotypic alterations, and metabolic disturbances at the metabolite and pathway levels. The PFAS mixture composition was selected based on epidemiological data, covering a broad concentration spectrum observed in diverse human populations. Phenotypic profiling by Cell Painting assay disclosed predominant effects of PFAS exposure on mitochondrial structure and function in both cell models as well as effects on F-actin, Golgi apparatus, and plasma membrane-associated measures. We employed comprehensive metabolic characterization using liquid chromatography combined with high-resolution mass spectrometry (LC-HRMS). We observed dose-dependent changes in the metabolic profiles, particularly in lipid, steroid, amino acid and sugar and carbohydrate metabolism in both cells as well as in cell media, with HepaRG cell line showing a stronger metabolic response. In cells, most of the bile acids, acylcarnitines and free fatty acids showed downregulation, while medium-chain fatty acids and carnosine were upregulated, while the cell media showed different response especially in relation to the bile acids in HepaRG cell media. Importantly, we observed also nonmonotonic response for several phenotypic features and metabolites. On the pathway level, PFAS exposure was also associated with pathways indicating oxidative stress and inflammatory responses. Taken together, our findings on PFAS-induced phenotypic and metabolic disruptions in hepatocytes shed light on potential mechanisms contributing to the broader comprehension of PFAS-related health risks.

1. Introduction

Per- and polyfluoroalkyl substances (PFAS) are industrial chemicals that are widely used in products such as food packaging, waterproof fabrics, firefighting foams, and nonstick pans. As persistent, bioaccumulating chemicals, they are widely spread in the environment, and they are also detected in human populations. Exposure to PFAS has been linked to numerous health issues including hepatotoxicity, developmental toxicity, and immunotoxicity, with main investigations covering the impacts of perfluorinated alkyl substances such as perfluorinated sulfonic acids and perfluorinated carboxylic acids (Ammitzbøll et al., 2019; Granum et al., 2013; Louisse et al., 2023; Yang et al., 2023; Jin et al., 2020; Bijland et al., 2011). In humans and animals, PFAS are known to enrich particularly in the liver, and several studies have shown that exposure to PFAS can lead to liver damage and metabolic alterations, particularly affecting hepatocytes as main functional cells of the liver (Louisse et al., 2023; Yang et al., 2023; Bijland et al., 2011). In the liver, PFAS exposure has been linked to changes in lipid metabolism,

* Corresponding author at: MTM Research Centre, School of Science and Technology, Örebro University, SE-701 82 Örebro, Sweden.
E-mail address: tuulia.hyotylainen@oru.se (T. Hyötyläinen).
[1] Equal contribution.

https://doi.org/10.1016/j.envint.2024.108820
Received 2 February 2024; Received in revised form 13 June 2024; Accepted 13 June 2024
Available online 17 June 2024

including disruptions in lipid accumulation and metabolism as well as lipid excretion pathways, potentially leading to steatotic liver disease (Louisse et al., 2023; Jin et al., 2020; Bijland et al., 2011; Addicks et al., 2023). PFAS exposure has also been associated with inflammation and oxidative stress as well as impaired glucose metabolism (Alderete et al., 2019; Cardenas et al., 2017; Christensen et al., 2019). Nevertheless, the relationship between PFAS exposure and hepatic lipid metabolism as well as the molecular mechanisms underlying these associations are still poorly understood.

As the liver is a crucial metabolic organ, any hepatic dysregulation of metabolism can potentially have major adverse health impacts at the organismal level. The majority of the hepatic metabolic functions are executed by hepatocytes, and thus, different types of hepatocyte models have been used in exposure studies. Indeed, *in vitro* studies are important in the investigation of the metabolic effects of exposure. Both human and animal-derived hepatocytes have been utilized in investigations of the impacts of PFAS on the liver metabolism, using different omics-based results as readouts of the effect. Most studies are based on changes at the transcriptome level, with changes translated into metabolic pathway level, while there are very few studies utilizing comprehensive metabolomics. By comparing different *in vitro* models at basal gene expression level, including HepG2 and HepaRG cell lines, primary human hepatocytes, and liver, it was shown that HepaRG have the closest resemblance of primary human hepatocytes and liver (Jennen et al., 2010). Particularly, related to bile acid metabolism, HepaRG correlate well with the human liver data (de Bruijn et al., 2022). Other transcriptomic analyses have also verified that HepaRG model may provide relevant data of hepatotoxic effects of PFASs (Louisse et al., 2023). The difference between the two cell lines is that the HepG2 cells are immortalized cell line derived from a liver biopsy of an adolescent male with hepatocellular carcinoma while HepaRG cells are derived from a hepatocellular carcinoma in an adult female. HepaRG cells are a bipotent progenitor cell line that can differentiate into both hepatocyte-like and biliary epithelial-like cells. More advanced hepatocyte models, such as human hepatocyte spheroids can also be used for the investigation of hepatic toxicity mechanisms of PFAS exposure, results demonstrating impaired peroxisomal β-oxidation and other lipid metabolic pathways after PFAS exposure (Yang et al., 2023; Addicks et al., 2023). Other studies have also utilized HepaRG human liver cells in PFAS exposure studies, with exposure resulting in an increase in triglyceride levels while triggering downregulation of genes involved in cholesterol biosynthesis (Louisse et al., 2023). A recent study investigated metabolomic and proteomic changes in primary human hepatocytes after exposure to a single concentration of either perfluorooctance sulfonic acid (PFOS) and its alternative 6:2 chlorinated polyfluorinated ether sulfonate (6:2Cl-PFESA), showing that the main changes were in lipid metabolism, particularly in glycerophospholipid metabolism (Li et al., 2023). Moreover, a recent study demonstrated that PFOS and perfluorooctanoic acid (PFOA) affect cell morphological phenotypes, especially mitochondria, endoplasmic reticulum, and nucleoli (Pierozan et al., 2023), verifying the use of high-content profiling in detecting PFAS bioactivity and early exposure fingerprints.

Here we investigated the phenotypic and metabolic impacts of mixture of PFAS exposure on two hepatocyte cell lines, HepaRG and HepG2, using a wide concentration exposure range mimicking the levels detected in different human populations. Also, the composition of the PFAS mixture, containing PFOS, PFOA, perfluorononanoic acid (PFNA), perfluorodecanoic acid (PFDA), and perfluorohexanesulfonic acid (PFHxS), was chosen based on their levels in human population. The goal was to compare the two hepatocyte models define the PFAS-related phenotypic fingerprints in human hepatocytes and to identify which metabolic pathways are dysregulated by the PFAS exposure. The composition of the PFAS mixture was selected based on the data from epidemiological studies. We performed high-content morphological profiling by Cell Painting assay and comprehensive metabolic screening of the exposed hepatocytes using LC-HRMS.

2. Materials and methods

2.1. Chemicals

All solvents were HPLC grade or LC-MS grade, from Honeywell (Morris Plains, NJ, USA), Fisher Scientific (Waltham, MA, USA) or Sigma-Aldrich (St. Louis, MO, USA). Mass spectrometry grade ammonium acetate and reagent grade formic acid were also from Sigma-Aldrich (St. Louis, MO, USA). The lipid standards were from Avanti Polar Lipids Inc. (Alabaster, AL, USA). ^{13}C-labeled PFAS internal standards (IS), ^{13}C-labeled performance standards, and native calibration standards (perfluorocarboxylic acids [PFCAs] and perflurosulfonic acids [PFSAs]) were purchased from Wellington Laboratories (Guelph, Ontario, Canada). One native performance standard, 7H-dodecafluoroheptanoic acid, was purchased from ABCR (Karlsruhe, Germany). Cholic acid (CA), chenodeoxycholic acid (CDCA), deoxycholic acid (DCA), dehydrocholic Acid (DHCA), glycocjolic acid (GCA), glyco chenodeoxycholic acid (GCDCA), lithocholic acid (LCA), taurocholic acid (TCA), taurochenodeoxycholic acid (TCDCA), taurodeoxycholic acid TDCA, taurodehydrocholic acid (TDHCA), taurohyocholic acid (THCA), taurohyodeoxycholic acid (THDCA), taurolithocholic acid (TLCA), and tauroursocholic acid (TUDCA) were obtained from Sigma-Aldrich (St. Luis, MO, USA), hyodeoxycholic acid (HDCA), hyocholic acid (HCA), murocholic acids α, β and ω (αMCA, βMCA, ωMCA), 7-oxohyodeoxycholic acid (7-oxo-HDCA), 7-oxodeoxycholic acid (7-oxo-DCA), 12-oxo lithocholic acid (12-oxo-LCA), tauromurocholic acid), murocholic acids α, β and ω (TαMCA, TβMCA, TωMCA), glycodehydrocholic Acid (GDHCA), glycohyocholic acid (GHCA), and glycohyodeoxycholic acid) GHDCA from Steraloids (Newport, RI, U.S.A), glycolithocholic acid (GLCA) and glycoursocholic acid (GUDCA) from Calbiochem (Gibbstown, NJ, U.S.A), and glycodeoxycholic acid (GDCA) and ursocholic acid (UDCA) from Fluka (Buchs, Switzerland). Internal standards CA-d4, LCA-d4, UDCA-d4, CDCA-d4, DCA-d4, GCA-d4, GLCA-d4, GUDCA-d4 and GCDCA-d4 were obtained from Qmx laboratories Ltd. (Essex, UK). For quality assurance (QA), standard reference material serum NIST SRM 1950 (for lipidomics and metabolomics) and 1957 (for PFAS and bile acids) was purchased from the National Institute of Standards and Technology (NIST) at the US Department of Commerce (Washington, DC, USA).

All PFAS compounds were purchased from Sigma Aldrich, with the following ordering numbers: PFOA – 77262, PFOS – 77282, PFNA – 394459, PFDA – 177,741 and PFHxS – 50929. For the exposure experiments, the mixture was made from five individual PFAS compounds as follows. They were first dissolved in methanol, and after combining all PFAS compounds into a mixture, methanol was evaporated under a nitrogen flow and exchanged with DMSO (99.9 %, Sigma Aldrich, Stockholm, Sweden) to reach the desired concentrations. A stock solution with all five compounds was prepared containing 5.20 mg/mL of PFOS, 3.12 mg/mL of PFOA, 1.32 mg/mL of PFHxS, 0.56 mg/mL of PFNA, and 0.68 mg/mL of PFDA. The individual exposure concentrations (Table 1) were then prepared by dilution of the stock solution in cell culture media, as described in 2.3. The purity of the PFAS compounds was as follows: PFOA 95 %, PFOS 98 %, PFNA 97 %, PFHxS $\geq$ 98.0 % and PFDA $\geq$ 98.0 %. The PFAS and their ratios were chosen based on their levels in human population. To further check the purity of the mixture, we analyzed the mixture separately using the UPLC-QTOFMS method described in 2.5.1. All PFAS compounds showed that the mixture contained also branched isomers of the PFAS (supplementary figure 1), and especially PFOS contained ca. 55 % of three branched isomers. For other PFAS, the branched isomers contributed less than ca. 10 % of the total amount.

2.2. Cell cultures

HepG2 human hepatic cell line from the American Type Culture Collection (ATCC; isolated from the male donor) was cultured in

Table 1
Exposure concentrations and concentrations measured in the hepatocytes containing 47.8 % PFOS, 28.7 % PFOA, 12.1 % PFHxS, 6.3 % PFDA, and 5.1 % PFNA. The PFAS concentrations in the cells have been measured for each biological replicate (n = 3) and for each technical replicate (n = 4 per exposure condition) for each exposure concentrations, normalized by the total protein count in the cells, as a surrogate for the number of cells. In the cells, the relative standard deviations were 28 % for PFOS, 21.3 % for PFOA, 37.5 % for PFHxS, 31.6 % for PFNA and 22.2 % for PFDA in HepG2 cells, and 31.9 % for PFOS, 19.0 % for PFOA, 36.5 % for PFHxS, 23.2 % for PFNA, and 22.8 % for PFDA in HepaRG cells.

Dose		Non treated	DMSO	1	2	3	4	5	6	7	8
PFAS total (μM)		0	0	0.02	0.22	1.12	2.24	4.49	8.98	13.46	22.44
PFAS (μM)	**PFOS**	0	0	0.010	0.105	0.535	1.071	2.146	4.292	6.434	10.726
	PFOA	0	0	0.006	0.063	0.321	0.643	1.289	2.577	3.863	6.440
	PFHxS	0	0	0.002	0.027	0.136	0.271	0.543	1.087	1.629	2.715
	PFNA	0	0	0.001	0.014	0.071	0.141	0.283	0.566	0.848	1.414
	PFDA	0	0	0.001	0.011	0.057	0.114	0.229	0.458	0.686	1.144
PFAS in HepG2 (μM /μg protein)	**PFOS***	0	0	0.002	0.014	0.052	0.111	0.307	0.870	1.063	1.905
	PFOA*	0	0	0.006	0.006	0.014	0.024	0.057	0.140	0.202	0.466
	PFHxS	0	0	0.005	0.008	0.031	0.067	0.159	0.439	0.603	1.448
	PFNA	0	0	0.002	0.014	0.052	0.111	0.307	0.870	1.063	1.905
	PFDA	0	0	0.001	0.002	0.005	0.010	0.021	0.038	0.043	0.054
PFAS in HepaRG (μM /μg protein)	**PFOS**	0	0	0.001	0.020	0.087	0.176	0.411	1.139	1.390	2.869
	PFOA	0	0	0.003	0.005	0.015	0.029	0.063	0.150	0.177	0.350
	PFHxS	0	0	0.000	0.002	0.006	0.010	0.025	0.060	0.073	0.138
	PFNA	0	0	0.000	0.001	0.004	0.010	0.022	0.053	0.061	0.114
	PFDA	0	0	0.000	0.005	0.020	0.039	0.079	0.167	0.178	0.287

Dulbecco's Minimum Essential Medium F-12 nutrient mixture (DMEM-F12 + GlutaMAX; Gibco, San Diego, CA) supplemented with 10 % (v/v) fetal bovine serum (FBS; Sigma), 10 U/mL penicillin and 10 μg/mL streptomycin (P/S; Gibco), and 1x non-essential amino acids (NEAA; Gibco). After reaching 70–90 % confluency, cells were detached with 0.5 % trypsin-EDTA (Gibco) and reseeded in new T75 cell culture flasks and kept at 37 °C with 5 % CO_2. HepG2 is commonly used in studies of lipid metabolism and hepatotoxicity (Pramfalk et al., 2016; Arzumanian et al., 2021).

Undifferentiated HepaRG® human hepatic cell line (BIOPREDIC, France; isolated from the female donor), also considered a surrogate for primary human hepatocytes (Guillouzo et al., 2007), was cultured in the basal hepatic cell medium supplemented with HepaRG® Growth Medium Supplement with antibiotics (BIOPREDIC, France). Cells were grown in T75 cell culture flasks until reaching 100 % confluency (usually 3–4 days). Later, cells were maintained in the same culture flask for an additional 14 days in order to promote differentiation into hepatocyte-like and biliary-like cells under DMSO-free conditions (Rose et al., 2022). Complete cell medium was refreshed every 2–3 days. The cells were maintained at 37 °C with 5 % CO_2 atmosphere.

2.3. Cell seeding, exposure, and sample collection

On day 1, cells were trypsinized and seeded in 24-well culture plates (VWR, Sweden) at the high density of 10^6 cells per well in the volume of 500 μL and incubated for an additional 24 h. On day 2, cells were exposed to PFAS mixtures set at 8 different concentrations. After 24-h exposure, 300 μL of the culture supernatant was aspirated and centrifuged at 10 000 g for 5 min. Afterwards, supernatants were transferred to new tubes and stored at −80 °C until extraction and analysis. Cells were gently detached by the cell scraper and centrifuged at 500 g for 5 min. Supernatant fraction was carefully removed, and cell pellets were stored at −80 °C until extraction and analysis. For each cell line, experiments included 4 technical replicates, and 3 independent experiments/biological replicates. PFAS stock solutions (0.02, 0.22, 1.12, 2.24, 4.49, 8.98, 13.46, and 22.44 μM) were prepared in DMSO (Sigma Aldrich, Sweden). After diluting mixture in the cell culture media, the final DMSO concentration in the wells was set at 0.1 %. Table 1. Shows the exposure rations of individual PFAS in the mixture. Cell culture media with 0.1 % DMSO (v/v) was used as a solvent control. In addition, a non-treated control was also included in the experimental setup. For metabolomic analyses, 12 individual samples/exposure concentration were used.

2.4. Cell Painting assay: exposure, imaging, and data analysis

Cell Painting assay was performed as previously described by (Bray et al., 2016) and (Alijagic et al., 2023). In brief, cells were seeded in CellCarrier Ultra 96-well black-walled microplates (PerkinElmer) in a final volume of 100 μL, excluding the outer wells to minimize the edge-effect. HepG2 cells were seeded at a density of 20 000 cells/well and HepaRG cells were seeded at density of 40 000 cells/well, respectively. Following day, additional 100 μL of cell media containing PFAS mixtures set at 8 different concentrations (see section 2.3 and Table 1) was added on top of the cells. The total volume in each well was 200 μL and the final DMSO concentration was always set at 0.1 %. After 24 h of exposure, Cell Painting protocol was applied. Cell media was discarded by inverting the plates and mitochondria were live-labelled with Mito-Tracker (Invitrogen; Thermo Fisher Scientific, Eugene, OR) in 30 μL of prewarmed culture medium and cells were incubated for 30 min at 37 °C at a 5 % CO_2 atmosphere. Afterwards, cells were fixed by adding 10 μL of 16 % paraformaldehyde (PFA) for 20 min at the room temperature. Following the fixation, solution was discarded by inverting the plate and cells were washed two times with PBS, and stained with 30 μL of the stain cocktail containing Hoechst 33,342 (Thermo Scientific), SYTO 14 green (Invitrogen), Concanavalin A/Alexa Fluor 488 (Invitrogen), Wheat Germ Agglutinin/Alexa Fluor 555 (Invitrogen) and Phalloidin/Alexa Fluor 568 (Invitrogen) and 0.1 % Triton X-100 in 0.1 % bovine serum albumin prepared in PBS. The concentration of each fluorescent stain is reported in Bray et al. (2016). After 30 min of staining and four washing steps, cells were imaged with the InCell 2200 HTS system (GE Healthcare; Uppsala, Sweden) using a 20 × objective. The z-offsets for each channel were fine-tuned by assessing randomly selected wells/fields across the microplates, aiming to obtain clear and focused images of the cell compartments of interest. In summary, nine images representing nine distinct fields of view in each well were captured across five different fluorescence channels: DNA (Hoechst 33342), mitochondria (MitoTracker), Golgi apparatus and plasma membrane (Wheat Germ Agglutinin), F-actin (Phalloidin), nucleoli and RNA (SYTO 14), and the endoplasmic reticulum (Concanavalin A/Alexa Fluor 488). Cell Painting experiments were performed twice with six technical replicates for each exposure condition. DMSO-free control was also included.

Morphological features were obtained using the image analysis software CellProfiler v. 4.2.1 (https://www.cellprofiler.org) (Stirling et al., 2021). CellProfiler was running illumination correction (JUMP_illum_LoadData_v1.cppipe) and analytical (JUMP_analysis_v3.cppipe) pipelines (https://github.com/broadinstitute/imaging-platform-pipelines/tree/master/JUMP_production). After the extraction of

morphological profiles, QC procedures, normalization, and feature selection were performed. Detailed explanation of QC procedures is given in (Alijagic et al., 2023). Normalization against DSMO control cells was employed for morphological profiles using the algorithm presented in (Bray et al., 2016). The total number of selected features was 3483 for HepG2 and 3456 for HepaRG cells. The self-developed Python scripts were used for the heatmap construction. MORPHEUS (https://software.broadinstitute.org/morpheus/), an online matrix visualization and analysis software, was used for profiling purposes and detection of significantly altered features by *t*-test.

2.5. LC-MS analysis

All samples were randomized before sample preparation and analysis. 12 replicate samples for each concentration were extracted and analyzed. The samples were analyzed using two parallel methods, one aimed at analysis of polar and semipolar metabolites and the second one for the analysis of lipids (Table 2). The cell pellets were first homogenized by adding 150 μL 0.9 % NaCl solution, after which the samples were vortex mixed and ultrasonicated for 3 min.

Two separate analyses were done, one covering PFAS and polar and semipolar metabolites and the second one covering lipidomics. Both analyses were done by an ultra-high-performance liquid chromatography quadrupole time-of-flight mass spectrometry (UHPLC-QTOFMS). Briefly, the UHPLC system used in this work was a 1290 Infinity II system from Agilent Technologies (Santa Clara, CA, USA). The system was equipped with a multi sampler (maintained at 10 °C), a quaternary solvent manager and a column thermostat (maintained at 50 °C). MassHunter B.06.01 software (Agilent Technologies, Santa Clara, CA, USA) was used for all data acquisition.

2.5.1. Analysis of PFAS, polar and semipolar metabolites

For analysis of bile acids, PFAS and polar metabolites, a combined target-non-target method for the analysis of semipolar metabolites and pollutants was used. 80 μL of cell homogenate or 80 μL cell media was extracted with 400 μL of cold MeOH/H_2O containing the internal standard mixture (Valine-d8, Glutamic acid-d5, Succinic acid-d4, Heptadecanoic acid, Lactic acid-d3, Citric acid-d4. 3-Hydroxybutyric acid-d4, Arginine-d7, Tryptophan-d5, Glutamine-d5, 1-D4-CA,1-D4-CDCA,1-D4-CDCA,1-D4-GCA,1-D4-GCDCA,1-D4-GLCA,1-D4-GUDCA,1-D4-LCA,1-D4-TCA, 1-D4-UDCA). The tube was vortexed and ultrasonicated for 3 min, followed by centrifugation (10,000 rpm, 5 min). After centrifuging, 350 μL of the upper layer of the solution was transferred to the LC vial and evaporated under the nitrogen gas to the dryness. After drying, the sample was reconstituted into 60 μl of MeOH: H2O (70:30) and kept at −80 °C until analysis.

Quantitation was done using 6-point calibration (PFOA C = 3.75–120 ng/mL, bile acids c = 20–640 ng/mL, polar metabolites c = 0.1 to 80 μg/mL). Quantification of other bile acids was done using the following compounds: Chenodeoxycholic acid (CDCA), Cholic acid (CA), Deoxycholic acid (DCA), Glycochenodeoxycholic acid (GCDCA), Glycocholic acid (GCA), Glycodehydrocholic acid (GDCA), Glycodeoxycholic acid (GDCA), Glycohyocholic acid (GHCA), Glycohyodeoxycholic acid (GHDCA), Glycolithocholic acid (GLCA), Glycoursodeoxycholic acid (GUDCA), Hyocholic acid (HCA), Hyodeoxycholic acid (HDCA), Litocholic acid (LCA), alpha-Muricholic acid (αMCA), Tauro-alpha-muricholic acid (T-α-MCA), Tauro-beta-muricholic acid(T-β-MCA), Taurochenodeoxycholic acid (TCDCA), Taurocholic acid (TCA), Taurodehydrocholic acid (THCA), Taurodeoxycholic acid (TDCA), Taurohyodeoxycholic acid (THDCA), Taurolithocholic acid (TLCA), Tauro-omega-muricholic acid (TωMCA) and Tauroursodeoxycholic acid (TDCA) and polar metabolites was done using alanine, citric acid, fumaric acid, glutamic acid, glycine, lactic acid, malic acid, 2-hydroxybutyric acid, 3-hydroxybutyric acid, linoleic acid, oleic acid, palmitic acid, stearic acid, cholesterol, fructose, glutamine, indole-3-propionic acid, isoleucine, leucine, proline, succinic acid, valine, asparagine, aspartic acid, arachidonic acid, glycerol-3-phosphate, lysine, methionine, ornithine, phenylalanine, serine and threonine. The curves had R values > 0.98 for most of the compounds. Identification was done based on in-house library (*m/z*, MS/MS, retention times) that is based on analysis of authentic standards.

Standard solutions extracted blanks (n = 3), pooled QC samples (n = 3, an aliquot of each sample pooled), in-house serum QC and NIST SRM 1950 (human plasma) were analyzed together with the samples. Identification was done based on in-house library with retention time and spectral data (level 1 identification, based on Metabolic Standard Initiative (Sumner et al., 2007). For pooled samples, identified metabolites that could be detected in both cell lines have average RSD in the pooled cell samples 20.4 % for HepG2 cells and 24.7 % for HepaRG cells. The relative standard deviation of the identified compounds was < 10 % for 38 % of the metabolites, <20 % for 25 % of the metabolites and < 30 % for 37 % of the metabolites%, and for the unidentified compounds the corresponding % were 11 % (<10 %), 41 % (<20 %) and 48 % (<30 %). For PFAS, the RSD was on average 9.6 %.

Table 2
LC-MS conditions for the two methods used in the study.

Conditions	Polar/semipolar compounds: Method 1	Lipidomics: Method 2
Injection volume	10 μl	1 μl
Column	C18 precolumn (Waters Corporation, Wexford, Ireland) and an inline filter, pore size 0,2 μm (Waters Corporation, Wexford, Ireland). + ACQUITY UPLC® BEH C18 column (2.1 mm × 100 mm, particle size 1.7 μm) by Waters (Milford, MA, USA)	C18 precolumn (Waters Corporation, Wexford, Ireland) and an inline filter, pore size 0,2 μm (Waters Corporation, Wexford, Ireland). + ACQUITY UPLC® BEH C18 column (2.1 mm × 100 mm, particle size 1.7 μm) by Waters (Milford, MA, USA)
Mobile phases	A H_2O:MeOH (v/v 70:30) with 2 mM ammonium acetate B MeOH with containing 2 mM ammonium acetate	A 10 mM ammonium acetate and 0.1 % Formic Acid in H_2O B Acetonitrile:Isopropanol (v/v 1:1) with 0.1 % Formic Acid and 10 mM ammonium acetate
Gradient	• 0–1.5 min: B was increased from 5 % to 30 % • 1.5–4.5 min, • B increased to 70 %; • 4.5–7.5 min, • B increased to 100 % and held for 5.5 min. • A post-time of 6 min	• 0–2 min, B was increased from 35 % to 80 % • 2–7 min, B increased to 100 % • 7–14 min, B was held at 100 %. • A post-time of 7 min
Flow rate	0.4 mLmin-1	0.4 mLmin-1
MS conditions	Dual ESI ionization source with capillary voltage 4.5 kV, nozzle voltage 1500 V, N2 pressure in the nebulized was 21 psi and the N2 flow rate and temperature as sheath gas was 11 Lmin-1 and 379 °C, respectively. Drying gas flow was set to 10 Lmin-1 and temperature to 150 °C. *m/z* range 100–1700 in negative ion mode.	Dual ESI ionization source with capillary voltage 3.64 kV, nozzle voltage 1500 V, N2 pressure in the nebulized was 21 psi and the N2 flow rate and temperature as sheath gas was 11 Lmin-1 and 379 °C, respectively. Drying gas flow was set to 10 Lmin-1 and temperature to 193 °C. *m/z* range 100–1700 in positive ion mode

2.5.2. Analysis of molecular lipids (lipidomics)

For lipidomics the samples were extracted using a modified version of the previously-published Folch procedure (Sen et al, 2022). In short, 150 μL of CHCl3: MeOH (2:1, v/v) containing the internal standards (c = 2.5 μg/mL) was added to 20 μL of sample homogenate. The standard solution contained the following compounds: 1,2-diheptadecanoyl-*sn*-glycero-3-phosphoethanolamine (PE(17:0/17:0)), N-heptadecanoyl-D-*erythro*-sphingosylphosphorylcholine (SM(d18:1/17:0)), N-heptadecanoyl-D-*erythro*-sphingosine (Cer(d18:1/17:0)), 1,2-diheptadecanoyl-*sn*-glycero-3-phosphocholine (PC(17:0/17:0)), 1-heptadecanoyl-2-hydroxy-*sn*-glycero-3-phosphocholine (LPC(17:0)) and 1-palmitoyl-d31-2-oleoyl-*sn*-glycero-3-phosphocholine (PC(16:0/d31/18:1)), were purchased from Avanti Polar Lipids, Inc. (Alabaster, AL, USA), and triheptadecanoylglycerol (TG(17:0/17:0/17:0)) was purchased from Larodan AB (Solna, Sweden). The samples were vortex mixed and incubated on ice for 30 min after which they were centrifuged (9400 × g, 3 min). 60 μL from the lower layer of each sample was then transferred to a glass vial with an insert and 60 μL of CHCl3: MeOH (2:1, v/v) was added to each sample. The samples were stored at −80 °C until analysis.

Calibration curves using 1-hexadecyl-2-(9Z-octadecenoyl)-*sn*-glycero-3-phosphocholine (PC(16:0e/18:1(9Z))), 1-(1Z-octadecenyl)-2-(9Z-octadecenoyl)-*sn*-glycero-3-phosphocholine (PC(18:0p/18:1(9Z))), 1-stearoyl-2-hydroxy-*sn*-glycero-3-phosphocholine (LPC(18:0)), 1-oleoyl-2-hydroxy-*sn*-glycero-3-phosphocholine (LPC(18:1)), 1-palmitoyl-2-oleoyl-*sn*-glycero-3-phosphoethanolamine (PE(16:0/18:1)), 1-(1Z-octadecenyl)-2-docosahexaenoyl-*sn*-glycero-3-phosphocholine (PC(18:0p/22:6)) and 1-stearoyl-2-linoleoyl-*sn*-glycerol (DG(18:0/18:2)), 1-(9Z-octadecenoyl)-*sn*-glycero-3-phosphoethanolamine (LPE(18:1)), N-(9Z-octadecenoyl)-sphinganine (Cer(d18:0/18:1(9Z))), 1-hexadecyl-2-(9Z-octadecenoyl)-*sn*-glycero-3-phosphoethanolamine (PE(16:0/18:1)) from Avanti Polar Lipids, 1-Palmitoyl-2-Hydroxy-*sn*-Glycero-3-Phosphatidylcholine (LPC(16:0)), 1,2,3 trihexadecanoalglycerol (TG(16:0/16:0/16:0)), 1,2,3-trioctadecanoylglycerol (TG(18:0/18:0/18:0) and 3β-hydroxy-5-cholestene-3-stearate (ChoE(18:0)), 3β-Hydroxy-5-cholestene-3-linoleate (ChoE(18:2)) from Larodan, were prepared to the following concentration levels: 100, 500, 1000, 1500, 2000 and 5000 ng/mL (in CHCl3:MeOH, 2:1, v/v) including 1250 ng/mL of each internal standard. The curves had R values > 0.99 for all lipids. Identification was done based on in-house library with retention time and spectral data (level 1 and 2 identification, based on Metabolic Standard Initiative). Lipid abbreviations are as follows: lipid headgroup followed by the fatty acyl composition (number of carbons in the fatty acyl, number of double bonds). Lipid headgroups: Ceramide (Cer), Sphingomyelin (SM), Phosphatidylcholine (PC), Alkylphosphatidylcholine (PC-O), Phosphatidylcholine plasmalogen (PC-P), Lysophosphatidylcholine (LPC), Phosphatidylethanolamine (PE), Akylphosphatidylethanolamine (PE-O), Phosphatidylethanolamine plasmalogen (PE-P), Lysophosphatidylethanolamine (LPE), Phosphatidylinositol (PI), Phosphatidylserine (PS), Cholesterol Ester (Ce), Diacylglycerol (DG), Triacylglycerol (TG).

Standard solutions extracted blanks (n = 3), pooled QC samples (n = 3, an aliquot of each sample pooled), in-house serum QC and NIST CRM 1950 (human plasma) were analyzed together with the samples. For pooled samples, identified lipids that could be detected in both cell lines have average RSD in the pooled cell samples 18.8 % for HepG2 cells and 26.1 % for HepaRG cells. Of the identified lipids, 29 % had RSD < 10 %, 21 % <20 % and 50 %<30 %, and for the unidentified compounds the corresponding RSD values were 28 % (<10 %), 36 % (<20 %) and 35 % (<30 %).

2.6. Data preprocessing

Processing of MS data was performed using the open-source software package MZmine 2.53 (Pluskal et al., 2010). The following steps were applied in this processing: (i) Crop filtering with a *m/z* range of 350 – 1200 *m/z* and an RT range of 2.0 to 12 min, (ii) Mass detection with a noise level of 750, (iii) Chromatogram builder with a minimum time span of 0.08 min, minimum height of 1000 and a *m/z* tolerance of 0.006 *m/z* or 10.0 ppm, (iv) Chromatogram deconvolution using the local minimum search algorithm with a 70 % chromatographic threshold, 0.05 min minimum RT range, 5 % minimum relative height, 1200 minimum absolute height, a minimum ration of peak top/edge of 1.2 and a peak duration range of 0.0– − 5.0, (v), Isotopic peak grouper with a *m/z* tolerance of 5.0 ppm, RT tolerance of 0.05 min, maximum charge of 2 and with the most intense isotope set as the representative isotope, (vi) Peak filter with minimum 8 data points, a FWHM between 0.0 and 0.2, tailing factor between 0.45 and 2.22 and asymmetry factor between 0.40 and 2.50, (vii) Join aligner with a *m/z* tolerance of 0.009 or 10.0 ppm and a weight for of 2, a RT tolerance of 0.15 min and a weight of 1 and with no requirement of charge state or ID and no comparison of isotope pattern, (viii) Peak list row filter with a minimum of 10 % of the samples (ix) Gap filling using the same RT and *m/z* range gap filler algorithm with an *m/z* tolerance of 0.009 *m/z* or 11.0 ppm, (x) Identification of lipids and metabolites using a custom database search with an *m/z* tolerance of 0.009 *m/z* or 10.0 ppm and a RT tolerance of 0.15 min, and (xi) Normalization using internal standards: For lipids: PE(17:0/17:0), SM(d18:1/17:0), Cer(d18:1/17:0), LPC(17:0), TG(17:0/17:0/17:0) and PC(16:0/d30/18:1)) for identified lipids and closest internal standard for the unknown lipids followed by calculation of the concentrations based on lipid-class concentration curves. For polar metabolites the following internal standards were used: Valine-d8, Glutamic acid-d5, Succinic acid-d4, Heptadecanoic acid, Lactic acid-d3, Citric acid-d4. 3-Hydroxybutyric acid-d4, Arginine-d7, Tryptophan-d5, Glutamine-d5, 1-D4-CA,1-D4-CDCA,1-D4-CDCA,1-D4-GCA,1-D4-GCDCA,1-D4-GLCA,1-D4-GUDCA,1-D4-LCA,1-D4-TCA, 1-D4-UDCA and closest internal standard for the unknown metabolites followed by calculation of the concentrations-based concentration curves. For data filtering, we have removed compounds that were present at blank samples (peak area > 5 times that of blank) and compounds that had RSD > 30 % in the pooled quality control samples. MS/MS data was done for the pooled quality control samples using auto MS/MS mode. The two cell lines were analyzed separately but the data preprocessing was done together. The data was adjusted by in-house pooled samples that were analyzed in both batches to correct the difference between the two batches.

2.7. Data analysis

Data analyses were conducted using Metaboanalyst 5.0 (Chong et al., 2019) and the R statistical programming language (version 4.1.2) (https://www.r-project.org/). In order to correct for heteroscedasticity, the exposure datasets were pre-processed by log10 transformation and scaling to zero mean and unit variance (autoscaled)as metabolomics data is not normally distributed. The statistical analyses included principal component analysis (PCA), analysis of variance (ANOVA), *t*-test and fold-change between controls and individual PFAS concentrations, Spearman correlations, and partial correlations between the PFAS and metabolites.

Pathway enrichment analysis was performed using the MetaboAnalyst 5.0 web platform with the Functional Analysis (MS Peaks) module (Pang et al. 2022 (Lu et al., 2022). This approach supports functional analysis of untargeted metabolomics data generated from high-resolution mass spectrometry. The pathway analysis was done with the data of the polar and semipolar metabolites, as the pathway analysis for lipidomics data is not sufficiently robust due to lack of exact structures of the lipids (fatty acid composition, including the position of the double bonds, cis/trans configuration). However, our polar/semipolar panel (Method 1) includes a large number of lipids, except for neutral lipids (CE, DG, TG) that are not covered either by sample preparation nor the negative ion mode. The input data for the pathway analysis comprised complete LC-HRMS data, i.e. both identified and unknown metabolites, obtained in negative ionization mode. First, we performed statistical analyses using *t*-test between control and each exposure

concentration between PFAS and polar metabolites, resulting in fold change, p values and FDR values. The whole input peak list, with peak names given as their numeric mass (*m/z*) values for putative annotation, and the statistical results with False Discovery Rate (FDR)-corrected p-values and t-score was used for the pathway analysis. Two algorithms were applied separately, namely, Mummichog and Gene Set Enrichment Analysis (GSEA) and two pathway libraries were used in the pathway analysis, namely human scale metabolic model MNF (from MetaboAnalyst Mummichog package) and Kyoto Encyclopedia of Genes and Genomes (KEGG) pathways for *Homo Sapiens* to determine the relative significance of the identified pathways (Li et al. 2020). The mass tolerance for the pathway analysis was set at 7 ppm, and we also used an advanced option to select representative adducts by removing isotopic adducts as these have been already removed in our data preprocessing step.

3. Results

3.1. Cell Painting unveils the phenotypic fingerprints of PFAS exposure

The exposure concentrations were chosen to reflect that of human exposure, both in terms of PFAS ratios in the mixture as well as related to the concentration range. Moreover, the maximum concentration was chosen to be lower than what might cause toxic effects. During the exposure, the cell viability was not altered in any significant manner. The solvent did not cause any significant effects on the phenotypic or metabolic profiles.

A non-targeted Cell Painting assay was used to detect (i) changes in morphological phenotypes associated with the PFAS exposure and (ii) differences between HepG2 and HepaRG phenotypic effects. The phenotypic profiling disclosed prominent changes across various subcellular sites upon exposure to the PFAS mixture. Either linear or non-

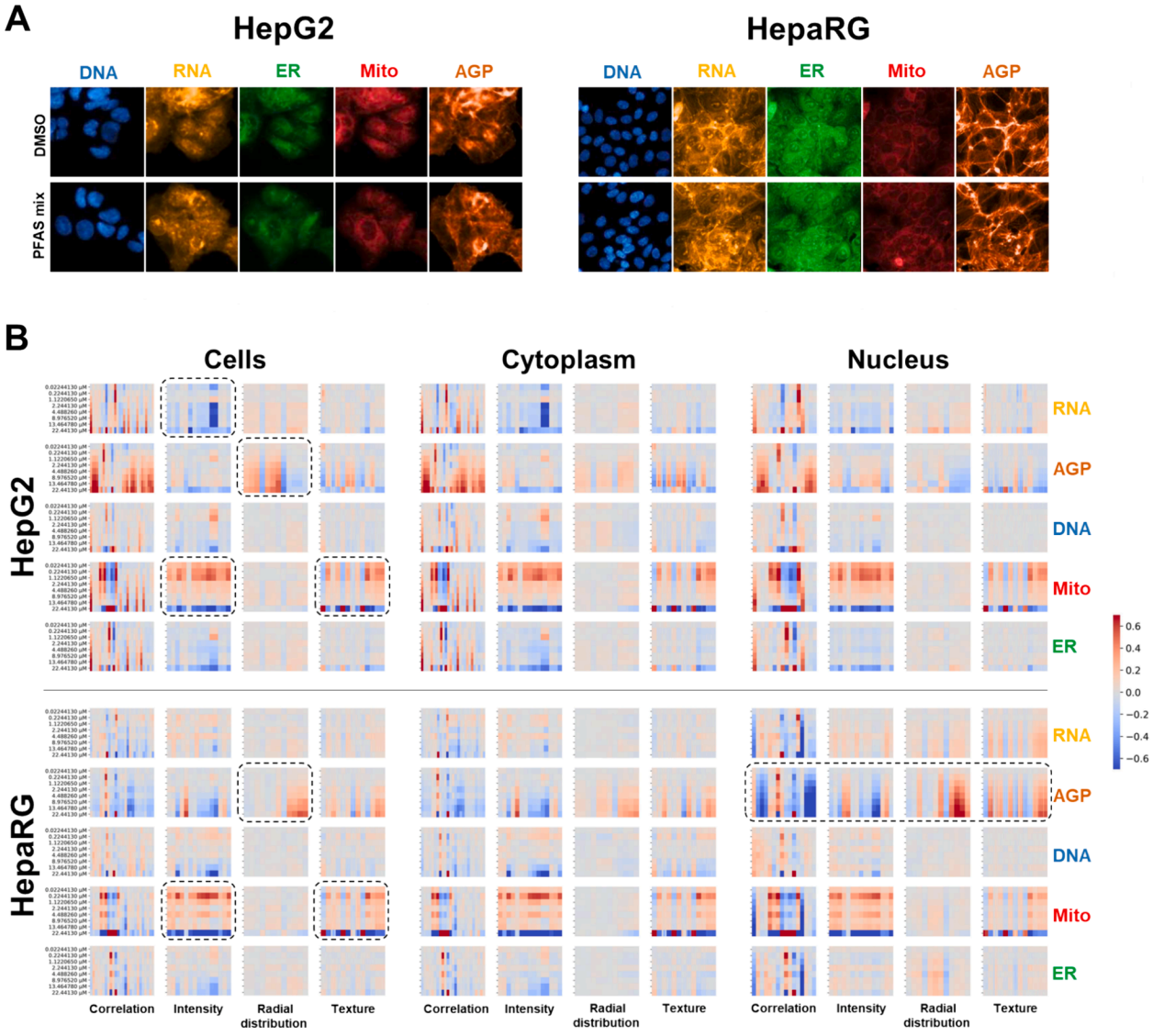

Fig. 1. Phenotypic profiling of PFAS-exposed hepatocytes by the Cell Painting assay. (A) Representative Cell Painting images of the HepG2 and HepaRG control (DMSO) and cells exposed to PFAS mixture (22.44 μM). All images were acquired at a 20 × magnification. (B) Heatmaps summarizing morphological features organized by compartment – cytoplasm, nuclei, and cell; by feature group – correlation, intensity, radial distribution, and texture; and by fluorescent channel – nuclei (DNA), actin cytoskeleton/Golgi apparatus/plasma membrane (AGP), endoplasmic reticulum (ER), RNA/nucleoli (RNA), and mitochondria (Mito). The number of displayed HepG2 features: correlation – 351, intensity – 243, radial distribution – 327, and texture – 2160. The number of displayed HepaRG features: correlation – 361, intensity – 241, radial distribution – 318, and texture – 2153. The colors represent fold change in each measured feature, with respect to the DSMO control cells. Columns display individual morphological features. Data were obtained from single-cell profiles distributed across six technical replicates (wells) distributed across two biological replicates (plates).

monotonic dose-dependent response was observed for a number of phenotypic features. Cell Painting labelling patterns of HepG2 and HepaRG cells and heatmaps summarizing the phenotypic profiles of control and PFAS-exposed cells are presented in Fig. 1. The overall comparison highlighted that similar feature clusters were affected by PFAS exposure both in HepG2 and HepaRG cells.

Features related to the mitochondrial (Mito), and AGP (actin, Golgi apparatus, and plasma membrane) phenotypes displayed the highest degree of changes in both cell types (Fig. 1**B**, dotted rectangles). These changes appeared to be interdependent as both cell types exhibited significant alterations ($p < 0.05$) in the feature subset *Correlation_Overlap_AGP_Mito*, possibly hinting at crosstalk between these subcellular structures in response to PFAS exposure. Notably, the highest PFAS concentration (22.44 μM) had a severe impact on the Mito reducing the large set of mitochondrial intensity- and texture-related measures. These changes may indicate impaired mitochondrial potential, resulting in reduced staining by MitoTracker. (Buckman et al., 2001) As the PFAS concentration decreased, the response became less evident. However, at the lowest PFAS concentrations (≤1.12 μM), the similar set of Mito features showed markedly opposite response and increase in a number of intensity- and texture-related measures. This suggests that PFAS may have opposite effects at lower concentrations, potentially unveiling intensified mitochondrial activity. Some of the Mito-related features significantly altered in both cell models were *Cells_Texture_InfoMeas2_Mito* and *Cells_RadialDistribution_RadialCV_mito_tubeness*. The feature *Cells_Intensity_MinIntensityEdge_Mito* was found altered in HepaRG, and *Cytoplasm_Texture_Entropy_Mito* in HepG2 cells, respectively. Moreover, AGP alterations exhibited a clear dose-dependent response, with HepaRG nuclear compartment being the most affected across all feature groups.

Interestingly, a small subset of RNA-related intensity features in the cytoplasmic compartment of HepG2 cells was found responsive to the PFAS, for example, *Cells_Intensity_MaxIntensity_RNA* or *Cytoplasm_Intensity_LowerQuartileIntensity_RNA*, whereas this response was not observed in HepaRG cells. The observed reduction in these RNA-related intensity features may imply a decreased RNA content within the cytoplasm in comparison to unexposed HepG2 cells. Limited changes in DNA and ER features in both cell models were detected mainly at the

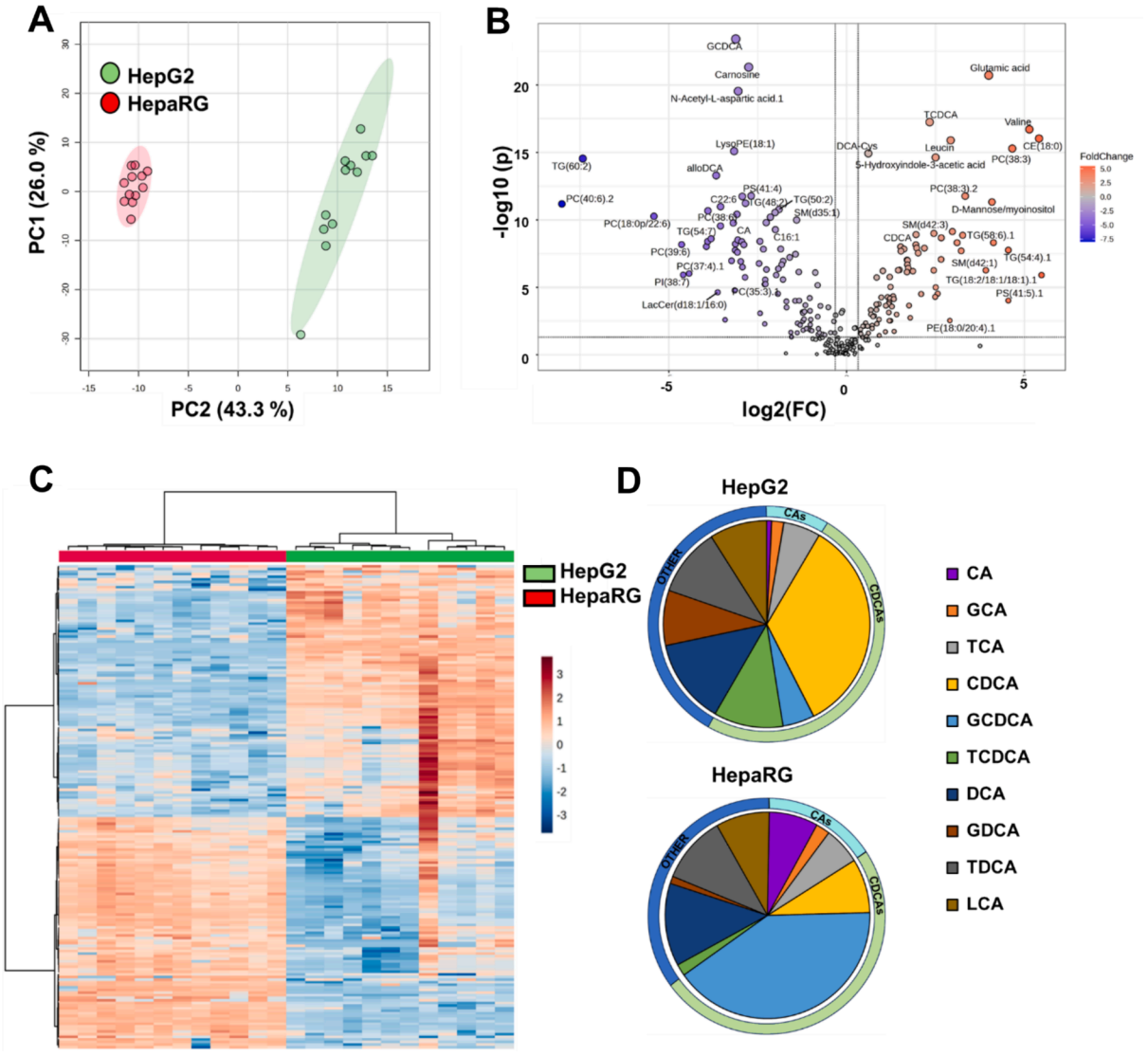

Fig. 2. Comparison of the non-treated HepG2 and HepaRG hepatocytes. (A) PCA of the metabolic profiles on HepG2 (green) and HepaRG (red), (B) volcano plot, showing that 180 metabolites were different between HepG2 and HepaRG (FC>±1.25, adj. $p < 0.05$), (C) heatmap of metabolome in the two cell lines, showing that the metabolic profiles have distinct patterns in HepG2 and HepaRG lines ($p < 0.05$), (D) bile acid pool composition (as % of the total bile acid concentration pool (ng/mL)) showing clear differences between the bile acid composition in the two cell lines. (For interpretation of the references to color in this figure legend, the reader is referred to the web version of this article.)

highest PFAS concentration. Regardless, features *Cells_Intensity_MinIntensityEdge_ER*, *Cells_RadialDistribution_FracAtD_ER* and *Cells_Intensity_MinIntensity_DNA* were found to be PFAS-responsive. A negative fold change in ER-related features compared to the control most likely indicates impaired ER membrane integrity and reduced concanavalin A binding to glycoproteins found in the ER membranes. (Alijagic et al., 2023) Interestingly, PFAS enlarged the overall size of both HepG2 and HepaRG cells as seen in the significant increase of the *Cytoplasm_AreaShape_Area* feature.

3.2. Metabolic profiles in the two hepatocyte lines show distinct differences

Based on the Cell Painting results indicating PFAS exposure

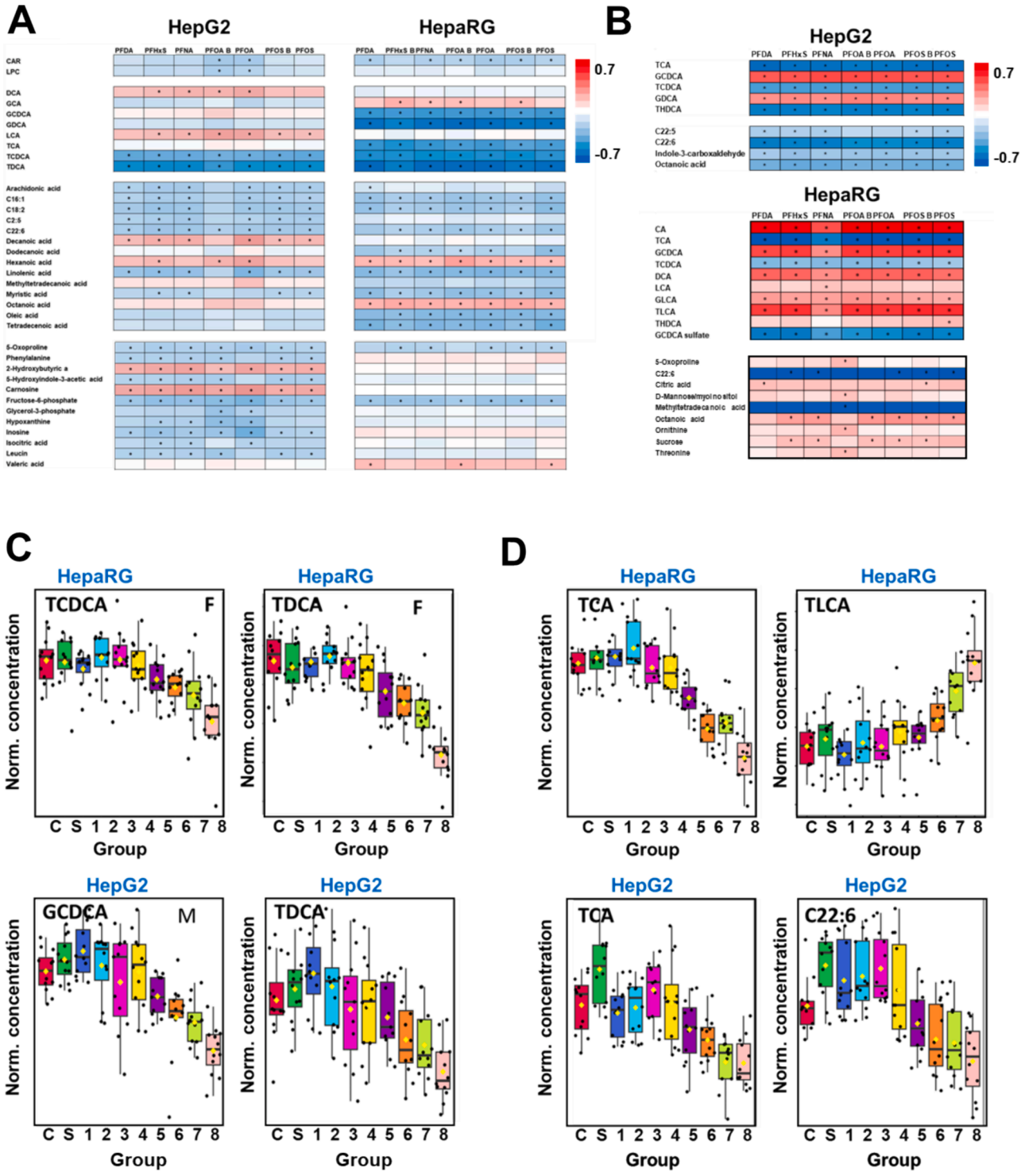

Fig. 3. (A) Correlation of PFAS exposure and lipid classes, bile acids, free fatty acids, amino acids and other polar metabolites in cells, only showing metabolites that show significant correlation with at least a single PFAS on either of the cell lines. (B) Correlation of PFAS exposure and bile acids, free fatty acids, amino acids, and other polar metabolites in supernatant, (C) examples of bile acids in HepG2 and HepaRG cells and (D) in the supernatant in HepG2 and HepaRG. * $p < 0.05$ (A and B), C ctrl, S solvent control. For exposure concentrations, see Table 1. The branched isomers of the PFOS and PFOA are denoted by PFOS_B and PFOA_B, respectively.

fingerprints in HepG2 and HepaRG cells, we have performed comprehensive metabolomic and lipidomic profiling to further identify metabolites and pathways affected by PFAS exposure (identified metabolites and their nomenclature shown in Supplementary Table 1). The solvent did not have any significant effect on the metabolic profiles. The two hepatocyte cell lines showed clear differences in their metabolic profiles at the level of individual lipids and metabolites (Fig. 2). The HepaRG cell line displayed less variation, something that was also evident from their growth. The HepaRG cells showed a more uniform growth trajectory compared to HepG2, suggesting less variable proliferation rates, and consequently, biomolecular composition. However, at the lipid class level, there were only minor differences, with only ether-linked PEs (PEo, PEp) showing significant differences (fold change [FC] = 1.7, p = 0.004). In the bile acid pool, there was a major difference between the two lines of hepatocytes, especially in the CDCA and GDCA percentage. While in both cell lines the CDCA and its conjugates represented ca 50 % of the total BA pool, in the HepaRG cell line unconjugated CDCA made up ca. 30 % of the total bile acid pool but only 8.5 % of the HepG2 hepatocyte pool. Glycine conjugated CDCA contributed 40.6 % in the HepG2 hepatocyte bile acid pool but only 5.0 % in the HepaRG cell line. The supernatants showed differences in the bile acid pool profiles, especially related to TDCA and TCDCA ratios: HepG2 cells 39 % of TCDCA and 8 % of TDCA while in HepaRG cell supernatant TDCDA contributes with 34 and TCDCA of 23 % of the total bile acid pool. This potentially reflects at least partially the differences in cell culture media.

3.3. PFAS exposure causes dose-dependent changes in the metabolome

We separately investigated the impact of PFAS exposure in cells and in the supernatant. PCA analysis showed no clear separation of the exposure groups in either of the cell lines, while supernatant (media) showed grouping in HepaRG cells (Supplementary Figure 2). In the cells, the PFAS exposure resulted in a significant suppression of conjugated primary bile acids (Fig. 3, Supplementary Table 2 and 3). At the level of lipid classes, PFAS showed suppressive impact on acyl-carnitines and lysophosphatidylcholines (LPCs), the latter only in HepG2. PFAS also suppressed the majority of the free fatty acids, with the exception of medium-chain fatty acids C6, C8, and C10, which all correspond to that of chain length in the most widespread PFAS. In addition, several amino acids and other polar metabolites were suppressed, with the impact stronger in the male hepatocyte line. Carnosine and 2-hydroxybutyric acid showed significant positive correlation in the HepG2 hepatocytes, while in the other cell line, no correlation was observed with the PFAS exposure. Valeric acid, on the other hand, showed positive association in the HepaRG but not in the HepG2 hepatocytes. In agreement with the Cell Painting results, particularly related to mitochondrial features, several metabolites also showed non-monotonic responses, with upregulated levels at lower exposure concentrations and downregulated levels at the highest exposure concentrations. (Fig. 3 C–D, Supplementary Figure 3).

In the supernatant, we primarily focused on the polar metabolites (Fig. 3**B**, Supplementary tables 4–5, **Supplementary** Figure 2). The PFAS exposure correlated strongly with several bile acids, with positive correlations for CA, GCDCA, DCA, LCA and its conjugates, while the taurine conjugates of both primary bile acids showed an opposite, negative correlation with PFAS. Free fatty acids did not show many associations with the PFAS in the supernatant, only C22:6 and methyltetradecanoic acid showed negative correlations and octanoic acid positive correlation with the PFAS.

Next, we investigated the intra-class partial correlations in the two cell lines, by considering PFAS as well as the following classes of metabolites: lipids, bile acid and polar metabolites (Fig. 4). The PFAS showed notable associations with metabolites, and there was also a clear difference between the associations between bile acids and lipids and in bile acids and polar metabolites. Importantly, we also observed that the two cell lines showed different types of interactions between the metabolites and PFAS, but also between the different metabolic classes.

3.4. Pathway analysis

We next performed Metabolic pathway analysis (Lu et al., 2022; Li et al., 2013) for both cell-lines, using the whole non-target data for cells in the analysis, and investigating each individual exposure concentration against solvent control (*t*-test, fold-change). The data input for the pathway analysis included mz values, retention times, fold change and p values. The pathway analyses showed that over 50 metabolic pathways were significantly dysregulated after PFAS exposure, in a dose-dependent manner (Fig. 5, Supplementary Tables 6–7). The two cell lines showed clearly distinct differences, with the female hepatocyte cell lines demonstrating clearly stronger impacts of the exposure. Overall, the main metabolic pathways that were dysregulated were related to lipid and amino acid metabolism as well as sugar and carbohydrate metabolism. Majority of the metabolites identified by the Pathway analysis in the dysregulated pathways showed downregulation, as shown in Supplementary Table 8, with the exposure group 7 in HepaRG

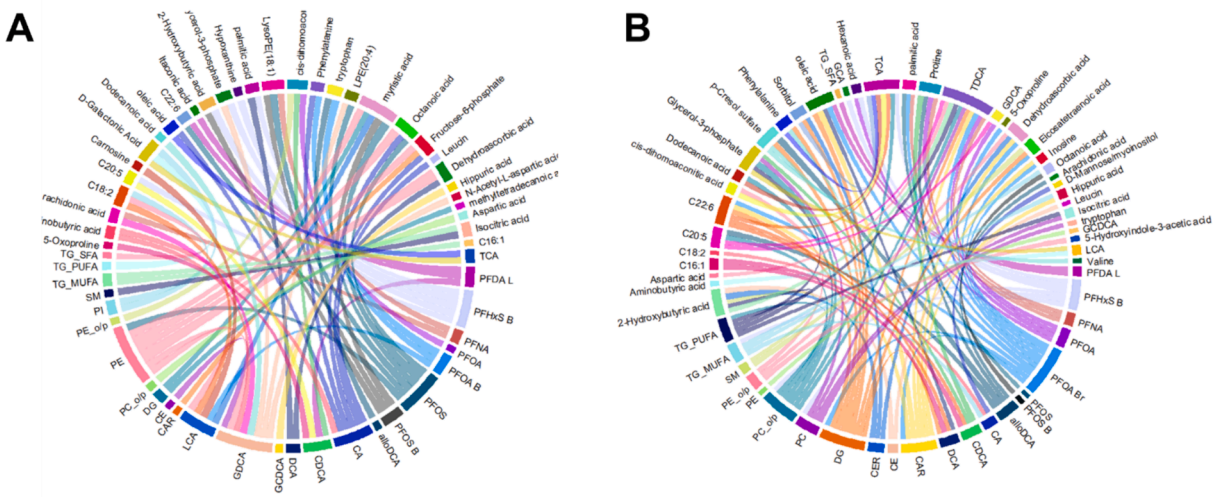

Fig. 4. Chord chart of significant partial intra-class correlations between PFAS and metabolites in (A) HepG2 and (B) HepaRG hepatocyte lines. Only significant correlations (p > 0.05) are shown, and intra-class correlations have been removed for clarity, as particularly PFAS and lipid classes showed strong intra-class correlations.

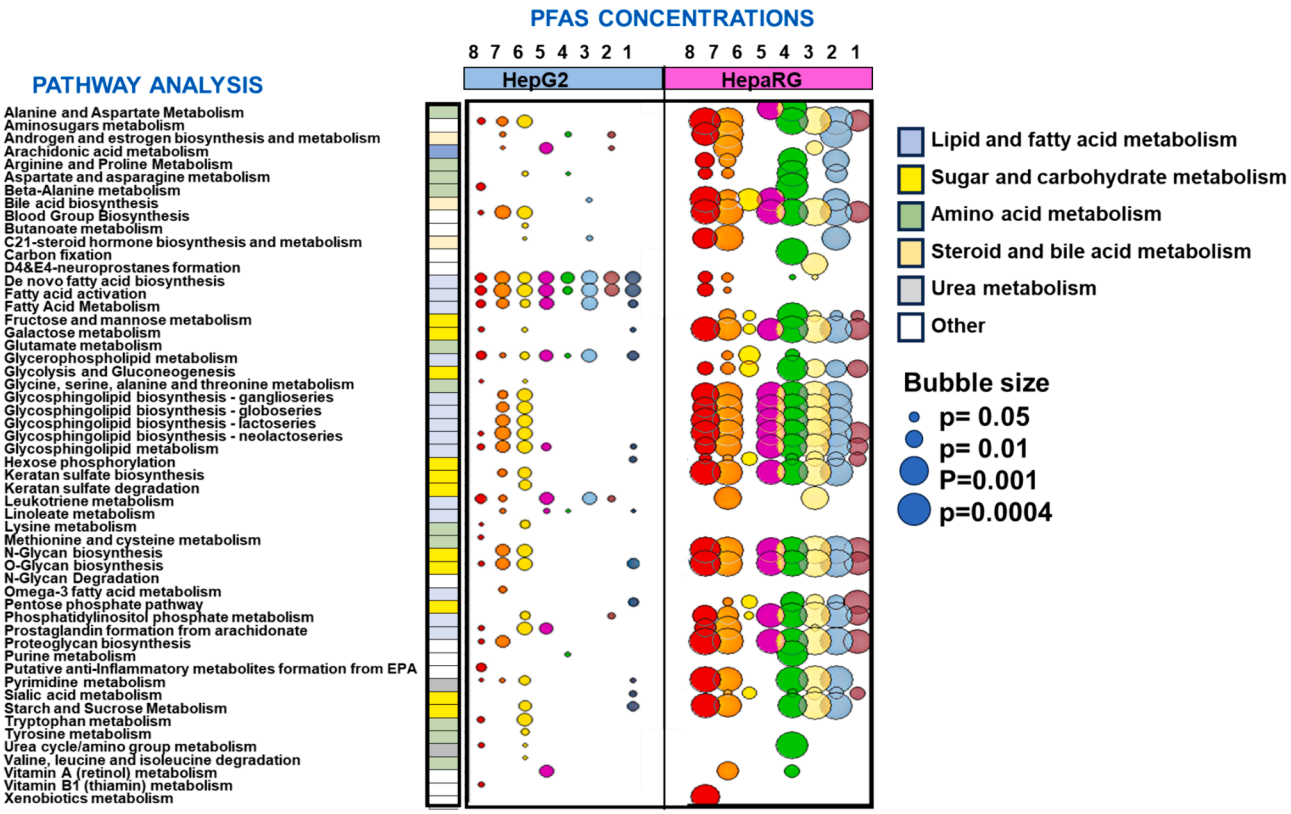

Fig. 5. Pathway analysis shows that the HepaRG hepatocytes (right) are showing stronger metabolic dysregulation after PFAS exposure compared with HepG2 (left). Bubble plot, with size of the bubble showing the p-value and the color is indicative of the exposure concentrations. For detailed information, see Supplementary tables 6–8.

as example, as this concentration level showed the strongest metabolic pathway dysregulation. In the pathway of C21-steroid hormone biosynthesis and metabolism, two of the metabolites were upregulated.

We also investigated the pathways using the supernatant, focusing on the HepaRG cells, as HepG2 cells showed too few significant changes in metabolites for reliable pathway analysis. The pathways that showed dysregulation in multiple concentration levels were Steroid hormone biosynthesis, Prostaglandin formation from arachidonate, Retinol metabolism and Androgen and estrogen biosynthesis and metabolism as well as Alanine, aspartate and glutamate metabolism.

4. Discussion

In this study, we investigated the impact of exposure to a mixture of PFAS in two hepatocyte cell lines. We observed dose-dependent changes in the phenotypic and metabolic profiles, with changes linked to disturbances in lipid, steroid, amino acid and sugar and carbohydrate metabolism. Importantly, we observed also non-monotonic response for several phenotypic features and metabolites, highlighting the importance of investigating a sufficiently large concentration range when investigating the biological responses of exposure. Moreover, as the differences were observed both in cells and in media, with very substantial changes particularly in bile acids in the media, both sample types should be included in the investigations.

Notably, we observed changes in the morphological phenotypes which closely mirror cells' state, outlining their functional requirements and the future behavior (Severin et al., 2022). Moreover, the changes showed similar response patterns to those observed in the metabolomics analyses, especially related to mitochondrial features. Phenotypic profiling by the Cell Painting assay disclosed that similar feature clusters were affected by PFAS exposure both in HepG2 and HepaRG hepatocytes. Overall, HepaRG cells appeared to be slightly more susceptible to phenotypic alterations due to the PFAS exposure than HepG2 cells, in line with the metabolomics data. Disruption of the mitochondrial structure and function were, most probably, a consequence of oxidative stress, as also suggested by the metabolic pathway analysis and in-line with the recent study by (Pierozan et al., 2023). A number of altered mitochondrial features, e.g., *Cells_Intensity_MinIntensityEdge_Mito* or *Cytoplasm_Texture_Entropy_Mito* suggest hyperpolarization, loss of membrane integrity, and fragmentation of mitochondria (Seal et al., 2022; Laber et al., 2023). Observed effects on mitochondria are consistent with previous mechanistic studies demonstrating that PFOS can lead to elevated mitochondrial ROS in hepatocytes *via* calcium overload. Consequently, ROS can cause alterations in mitochondrial membrane potential and membrane permeability, which correlates with the effects on the mitochondrial outer membrane observed in the Cell Painting (Xiaopeng and Jin, 2023). Additionally, ROS released from damaged mitochondria further diffuse into lysosomes, producing highly reactive hydroxyl radicals that lead to lipid peroxidation (Wang et al., 2022). This can further activate different inflammatory response pathways, e.g., mt-DNA-mediated NLRP3 or NF-κB/TNF-α-mediated signaling pathway (Xiaopeng and Jin, 2023; Han et al., 2018). Interestingly, finding that the feature *Cytoplasm_Intensity_LowerQuartileIntensity_RNA* was PFAS-responsive in HepG2 cells may have a number of biological implications including cell cycle, PIK3CA signaling, metabolism, proteasome activity, and Endoplasmic Reticulum (ER) stress (Seal et al., 2024:mbcE23080298.). *LowerQuartileIntensity* describes the pixel intensity value below which 25 % of the pixels within an object exhibit lower intensity values. In addition, correlated intensity changes between AGP and Mito objects, observed in both cell models (for example feature subset *Correlation_Overlap_AGP_Mito*), previously were found associated with several cellular processes including DNA damage, RTK signaling that regulates systemic glucose and lipid metabolism (Zhao et al., 2020), and Hippo signaling pathway which has multiple

points of crosstalk with the lipid metabolism (Seal et al., 2024: mbcE23080298.; Ibar and Irvine, 2020). Finding that PFAS exposure increased overall size of both cell lines may potentially have a number of biological implications. For example, the augmentation in the average size of hepatocytes, known as hepatocellular hypertrophy, resulting from chemical toxicity and/or the activation of PPARα (peroxisome proliferator-activated receptor alpha), a known target of PFAS (Evans et al., 2022), may underscore profound changes in oxidative status, fatty acid metabolism, and energy production of hepatocytes (Hall et al., 2012). In addition, PFAS exposure induced alterations in the AGP-related features, especially in the nuclear compartment of HepaRG cells. This finding agrees with the study by Behr et al. (2020) (Behr et al., 2020), which reported that PFOA or PFOS exposure induces disorganization of the F-actin cytoskeleton and a structural redistribution of the tight-junctional protein ZO-1 in HepaRG cells. Overall, Cell Painting results enabled identification of phenotypic changes, providing context for the interpreting subsequent metabolic alterations in hepatocytes exposed to PFAS.

On the pathway level, PFAS exposure was associated with pathways indicating oxidative stress and inflammatory responses (Prostaglandin formation from arachidonate, Arachidonic acid metabolism). While our target list included only a few metabolites in these pathways, the Metabolic pathway analysis tool was able to pick additional metabolites in these pathways, however, we could not verify their identity due to absence of authentic standards., while putative identification was possible for several of the metabolites. Dysregulation of multiple glycerosphingolipid (GSL) pathways by the PFAS exposure can also indicate hepatic oxidative stress (Apostolopoulou et al., 2018). GSLs act as second messengers in several cellular functions, such as in proliferation, adhesion migration, autophagy, apoptosis, and mitochondrial function in the cells, and thus, dysregulation in GSL can indicate adverse impacts in these key cellular functions. Dysregulation in GSL has also been linked with type 2 diabetes and metabolic syndrome as well as in drug-induced liver damage (Balram et al., 2022; Gai et al., 2023). This observation is further reinforced by the dysregulation of several key metabolic pathways related to sugar and carbohydrate metabolism by the PFAS, which is also in line with previous studies in experimental models and in epidemiological studies (Alderete et al., 2019; Cardenas et al., 2017; Donat-Vargas et al., 2019; Sun et al., 2018; He et al., 2018; Lind et al., 2014).

On the level of individual metabolites, bile acids showed strong dysregulation, however, the changes were not monotonic, with several metabolites showing either U-shaped or inverted U-shaped response patterns, suggesting that at low PFAS doses the metabolic responses are opposite to those observed at high doses. Our findings are in agreement with studies in animal models which have reported non-monotonic response pattern between PFAS exposure and profiles of multiple amino acids (Kariuki and E.G., Lankadurai, B.P., Simpson, A.J., Simpson, M.J. , 2017) as well as fatty acids and lipids (Geng et al., 2019). This type of non-linear response could be due hormesis, the over-compensation of different adaptive responses through cellular stress (Kim et al., 2018; Rossnerova et al., 2020). It has been suggested that hormesis could explain the findings showing that disease risk does not increase linearly with increasing dose of chemicals, but often tends to plateau or even decrease with increasing dose (Kim et al., 2018). This clearly demonstrates the necessity to investigate a range of exposure concentrations, as single dose experiments may fail to catch the relevant changes.

While we observed similarities in the metabolic responses after PFAS exposure in the HepG2 and HepaRG cell lines, there were also clear differences between the two cell lines. In terms of cholesterol and bile acid metabolism particularly, it has been stated that in HepaRG cells are very similar to primary hepatocytes and the expression of CYP enzymes and nuclear receptors involved in bile acid metabolism is close to the pattern of human primary hepatocytes (Rogue et al., 2012). In HepG2, genes involved in common metabolic processes, including CYP450s, have been shown to be underexpressed in comparison to HepaRG (Jennen et al., 2010). PFAS, on the other hand, have been shown to mediate metabolic impacts through multiple CYPs (Zhang et al., 2018), particularly related to impact of PFAS on bile acid metabolism, and as expected, the PFAS impact on bile acids was stronger in the HepaRG cells while the changes were not as clear in the HepG2 cells. At a higher dose, bile acids were downregulated by the PFAS, in line with reported data showing that CYP7A1, the key enzyme of bile acid synthesis, is suppressed by PFAS (Zhang et al., 2018). Our results agree well with previous studies suggesting that the HepaRG cell line is a better model for toxicity studies than to the HepG2 cell line (Jennen et al., 2010; de Bruijn et al., 2022; Rogue et al., 2012; Mesnage et al., 2018). Our results show stronger metabolic response in HepaRG cells after the exposure, with responses resembling those observed in human studies, agreeing with the data showing that this cell line possess metabolic activities that closely resemble primary human hepatocytes. Indeed, HepaRG cells can be differentiated into hepatocyte-like cells, acquiring functions and morphology similar to primary hepatocytes. This differentiation process enhances their metabolic activity and makes them more physiologically relevant for toxicological studies.

Interestingly, we could also detect secondary bile acids in the hepatocytes, such as lithocholic acid (LCA) as well as deoxycholic acid (DCA), both in the cells as well as in the supernatant. We also observed positive correlation of the LCA and DCA with PFAS exposure in HepaRG cells, while in the HepaRG line, we observed strong positive correlation between PFAS and both the glycine and taurine conjugated LCA as well as with DCA in the supernatant. The changes observed in the supernatant indicate that the hepatocytes response to the exposure by change in excreting patterns of these metabolites. In the HepaRG cells, PFAS were positively correlated with the glycine conjugated DCA. LCA is considered to be hepatotoxic, however, it has also been suggested to have anti-inflammatory effects at certain conditions (Sheng et al., 2022). We have previously observed in both human studies and in animal models positive association between PFAS exposure and LCA and its conjugates (Sen et al., 2022). While LCA is traditionally classified as secondary bile acid, its presence in hepatocytes has been reported also previously (Shiffka et al., 2020). It has been hypothesized that the production of secondary bile acids is due to the accumulation of unconjugated CA and CDCA within the cells, leading to insufficient conjugation and export and further dihydroxylation of these bile acids, which is likely performed by the same enzymes that rehydroxylate LCA and DCA in the normal liver, as this enzymatic reaction is reversible (Shiffka et al., 2020). Moreover, as we observed a clear PFAS exposure-associated increase of these bile acids in the media, they must have been synthesized by hepatocytes.

Overall, the metabolic changes we observed are in agreement with previous studies that have investigated PFAS associated metabolic changes in hepatocytes (Li et al., 2023; Behr et al., 2020). Down-regulation of the primary bile acids is in line with a recent study in HepaRG cells (Behr et al., 2020), where exposure to PFOS and PFOA were shown to trigger changes in genes regulating bile acid metabolism and the primary bile acids both in the cells as well as in the supernatant, pointing towards a feedback loop to prevent bile acid accumulation.

Our results are in several aspects in-line with those obtained in human epidemiological studies, or with animal models with PFAS-associated decrease in hepatic bile acids (Sen et al., 2022; McGlinchey, 2019; Sinioja et al., 2022; Sinisalu et al., 2021). However, there were also some major differences. We have shown earlier that PFAS exposure in humans is associated with sex-specific changes in the liver lipidome, with females showing positive association between PFAS and lipotoxic hepatic lipids while in males, inverse associations were observed (Sen et al., 2022), with similar impact verified in mice model (McGlinchey, 2019; Sinioja et al., 2022). However, in the current study, we observed only relatively low association between PFAS and lipids. This suggests, as we have earlier hypothesized, that a significant part of the impacts of PFAS are not direct, but are mediated by changes in gut microbial metabolites, such as secondary bile acids.

In conclusion, our data showed that PFAS causes dose-dependent, non-monotonic responses on cell phenotypic profiles and multiple metabolites, particularly linked with bile acid and glucose metabolism, as well as on pathways indicating oxidative stress and inflammatory responses. Moreover, our results demonstrated that PFAS exposure, probably as a consequence of the oxidative stress, mediates effects on structure and function of mitochondria, cytoskeleton, and lipid-rich membranes. Together, these data demonstrate that the synergy of metabolomic and phenotypic profiling in different hepatocyte models yield cellular signatures of PFAS exposure. When compared with data on animal models and epidemiological studies, there are clear indicators that the cellular models cannot fully capture indirect impacts on the metabolism, with these impacts being mediated, e.g., by the impact of PFAS exposure on gut microbiotaurur results show that is important to study the changes both in the cells, but also in the media, as strong changes were observed in the media, suggesting that the hepatocytes response to exposure be excreting specific metabolites, particularly bile acids to the media. Our study also highlights the importance of studying a sufficiently large concentration range of exposures, due to the non-monotonic response.

CRediT authorship contribution statement

Andi Alijagic: Writing – review & editing, Writing – original draft, Visualization, Validation, Resources, Project administration, Methodology, Investigation, Funding acquisition, Formal analysis, Data curation. **Lisanna Sinisalu:** Writing – review & editing, Methodology. **Daniel Duberg:** Writing – review & editing, Methodology. **Oleksandr Kotlyar:** Writing – review & editing, Methodology. **Nikolai Scherbak:** Writing – review & editing, Methodology. **Magnus Engwall:** Writing – review & editing, Methodology. **Matej Orešič:** Writing – review & editing, Funding acquisition, Conceptualization. **Tuulia Hyötyläinen:** Writing – review & editing, Writing – original draft, Visualization, Validation, Supervision, Resources, Project administration, Methodology, Investigation, Funding acquisition, Formal analysis, Conceptualization.

Declaration of competing interest

The authors declare the following financial interests/personal relationships which may be considered as potential competing interests: [Tuulia Hyotylainen reports financial support was provided by Swedish Research Council. Tuulia Hyotylainen reports financial support was provided by Novo Nordisk Foundation. Tuulia Hyotylainen reports financial support was provided by European Union. Magnus Engwall reports financial support was provided by Swedish Knowledge Foundation. If there are other authors, they declare that they have no known competing financial interests or personal relationships that could have appeared to influence the work reported in this paper].

Data availability

Data will be made available on request.

Acknowledgments

This study was supported by the Swedish Research Council (grants no. and 2020-03674 and 2016-05176 to T.H and M.O), Formas (grant no. 2019-00869 to T.H and M.O), Novo Nordisk Foundation (Grants no. NNF20OC0063971 and NNF21OC0070309 to T.H. and M.O.), and by the “Investigation of endocrine-disrupting chemicals as contributors to progression of metabolic dysfunction-associated steatotic liver disease” (EDC-MASLD) consortium funded by the Horizon Europe Program of the European Union under Grant Agreement 101136259 (to MO and TH). The study was also partially supported by grants from the Swedish Knowledge Foundation (Grants. no. 20160019; 20190107; 20220122). The authors would like to thank Adil Boustani for providing the images of hepatocytes.

Appendix A. Supplementary data

Supplementary data to this article can be found online at https://doi.org/10.1016/j.envint.2024.108820.

References

Addicks, G.C., Rowan-Carroll, A., Reardon, A.J.F., Leingartner, K., Williams, A., Meier, M.J., Moffat, I., Carrier, R., Lorusso, L., Wetmore, B.A., et al., 2023. Per- and polyfluoroalkyl substances (PFAS) in mixtures show additive effects on transcriptomic points of departure in human liver spheroids. Toxicol. Sci. 194 (1), 38–52.

Alderete, T.L., Jin, R., Walker, D.I., Valvi, D., Chen, Z., Jones, D.P., Peng, C., Gilliland, F. D., Berhane, K., Conti, D.V., et al., 2019. Perfluoroalkyl substances, metabolomic profiling, and alterations in glucose homeostasis among overweight and obese Hispanic children: a proof-of-concept analysis. Environ. Int. 126, 445–453.

Alijagic, A., Scherbak, N., Kotlyar, O., Karlsson, P., Wang, X., Odnevall, I., Benada, O., Amiryousefi, A., Andersson, L., Persson, A., et al., 2023. A Novel nanosafety approach using cell painting, metabolomics, and lipidomics captures the cellular and molecular phenotypes induced by the unintentionally formed metal-based (Nano) particles. Cells. 12 (2).

Alijagic, A., Kotlyar, O., Larsson, M., Salihovic, S., Hedbrant, A., Eriksson, U., Karlsson, P., Persson, A., Scherbak, N., Färnlund, K., et al., 2023. Immunotoxic, genotoxic, and endocrine disrupting impacts of polyamide microplastic particles and chemicals. Environ. Int. 183, 108412.

Ammitzbøll, C., Börnsen, L., Petersen, E.R., Oturai, A.B., Søndergaard, H.B., Grandjean, P., Sellebjerg, F., 2019. Perfluorinated substances, risk factors for multiple sclerosis and cellular immune activation. J. Neuroimmunol. 330, 90–95.

Apostolopoulou, M., Gordillo, R., Koliaki, C., Gancheva, S., Jelenik, T., De Filippo, E., Herder, C., Markgraf, D., Jankowiak, F., Esposito, I., et al., 2018. Specific hepatic sphingolipids relate to insulin resistance, oxidative stress, and inflammation in nonalcoholic steatohepatitis. Diabetes Care 41 (6), 1235–1243.

Arzumanian, V.A., Kiseleva, O.I., Poverennaya, E.V., 2021. The curious case of the HepG2 cell line: 40 years of expertise. Int. J. Mol. Sci. 22 (23).

Balram, A., Thapa, S., Chatterjee, S., 2022. Glycosphingolipids in diabetes, oxidative stress, and cardiovascular disease: prevention in experimental animal models. Int. J. Mol. Sci. 23 (23).

Behr, A.-C., Kwiatkowski, A., Ståhlman, M., Schmidt, F.F., Luckert, C., Braeuning, A., Buhrke, T., 2020. Impairment of bile acid metabolism by perfluorooctanoic acid (PFOA) and perfluorooctanesulfonic acid (PFOS) in human HepaRG hepatoma cells. Arch Toxicol.

Bijland, S., Rensen, P.C., Pieterman, E.J., Maas, A.C., van der Hoorn, J.W., van Erk, M.J., Havekes, L.M., Willems van Dijk, K., Chang, S.C., Ehresman, D.J., et al., 2011. Perfluoroalkyl sulfonates cause alkyl chain length-dependent hepatic steatosis and hypolipidemia mainly by impairing lipoprotein production in APOE*3-Leiden CETP mice. Toxicol. Sci. 123 (1), 290–303.

Bray, M.A., Singh, S., Han, H., Davis, C.T., Borgeson, B., Hartland, C., Kost-Alimova, M., Gustafsdottir, S.M., Gibson, C.C., Carpenter, A.E., 2016. Cell Painting, a high-content image-based assay for morphological profiling using multiplexed fluorescent dyes. Nat. Protoc. 11 (9), 1757–1774.

Buckman, J.F., Hernández, H., Kress, G.J., Votyakova, T.V., Pal, S., Reynolds, I.J., 2001. MitoTracker labeling in primary neuronal and astrocytic cultures: influence of mitochondrial membrane potential and oxidants. J. Neurosci Methods 104 (2), 165–176.

Cardenas, A., Gold, D.R., Hauser, R., Kleinman, K.P., Hivert, M.-F., Calafat, A.M., Ye, X., Webster, T.F., Horton, E.S., Oken, E., 2017. Plasma concentrations of per- and polyfluoroalkyl substances at baseline and associations with glycemic indicators and diabetes incidence among high-risk adults in the diabetes prevention program trial. Environ. Health Perspect. 125 (10), 107001.

Chong, J., Wishart, D.S., Xia, J., 2019. Using metaboanalyst 4.0 for comprehensive and integrative metabolomics data analysis. Nucleic Acids Res. 68 (1), e86.

Christensen, K.Y., Raymond, M., Meiman, J., 2019. Perfluoroalkyl substances and metabolic syndrome. Int. J. Hyg. Environ. Health 222 (1), 147–153.

de Bruijn, V.M.P., Wang, Z., Bakker, W., Zheng, W., Spee, B., Bouwmeester, H., 2022. Hepatic bile acid synthesis and secretion: comparison of in vitro methods. Toxicol Lett. 365, 46–60.

Donat-Vargas, C., Bergdahl, I.A., Tornevi, A., Wennberg, M., Sommar, J., Kiviranta, H., Koponen, J., Rolandsson, O., Åkesson, A., 2019. Perfluoroalkyl substances and risk of type II diabetes: a prospective nested case-control study. Environ. Int. 123, 390–398.

Evans, N., Conley, J.M., Cardon, M., Hartig, P., Medlock-Kakaley, E., Gray Jr., L.E., 2022. In vitro activity of a panel of per- and polyfluoroalkyl substances (PFAS), fatty acids, and pharmaceuticals in peroxisome proliferator-activated receptor (PPAR) alpha, PPAR gamma, and estrogen receptor assays. Toxicol. Appl. Pharmacol. 449, 116136.

Gai, Z., Samodelov, S.L., Alecu, I., Hornemann, T., Grove, J.I., Aithal, G.P., Visentin, M., Kullak-Ublick, G.A., 2023. Plasma sphingoid base profiles of patients diagnosed with intrinsic or idiosyncratic drug-induced liver injury. Int. J. Mol. Sci. 24 (3).

Geng, D., Musse, A.A., Wigh, V., Carlsson, C., Engwall, M., Orešič, M., Scherbak, N., Hyötyläinen, T., 2019. Effect of perfluorooctanesulfonic acid (PFOS) on the liver

lipid metabolism of the developing chicken embryo. Ecotoxicol Environ. Saf. 170, 691–698.
Granum, B., Haug, L.S., Namork, E., Stolevik, S.B., Thomsen, C., Aaberge, I.S., van Loveren, H., Lovik, M., Nygaard, U.C., 2013. Pre-natal exposure to perfluoroalkyl substances may be associated with altered vaccine antibody levels and immune-related health outcomes in early childhood. J. Immunotoxicol 10 (4), 373–379.
Guillouzo, A., Corlu, A., Aninat, C., Glaise, D., Morel, F., Guguen-Guillouzo, C., 2007. The human hepatoma HepaRG cells: a highly differentiated model for studies of liver metabolism and toxicity of xenobiotics. Chem. Biol. Interact 168 (1), 66–73.
Hall, A.P., Elcombe, C.R., Foster, J.R., Harada, T., Kaufmann, W., Knippel, A., Küttler, K., Malarkey, D.E., Maronpot, R.R., Nishikawa, A., et al., 2012. Liver hypertrophy: a review of adaptive (adverse and non-adverse) changes–conclusions from the 3rd International ESTP Expert Workshop. Toxicol. Pathol 40 (7), 971–994.
Han, R., Hu, M., Zhong, Q., Wan, C., Liu, L., Li, F., Zhang, F., Ding, W., 2018. Perfluorooctane sulphonate induces oxidative hepatic damage via mitochondria-dependent and NF-κB/TNF-α-mediated pathway. Chemosphere 191, 1056–1064.
He, X., Liu, Y., Xu, B., Gu, L., Tang, W., 2018. PFOA is associated with diabetes and metabolic alteration in US men: national health and nutrition examination survey 2003–2012. Sci. Total Environ. 625, 566–574.
Ibar, C., Irvine, K.D., 2020. Integration of hippo-YAP signaling with metabolism. Dev Cell 54 (2), 256–267.
Jennen, D.G.J., Magkoufopoulou, C., Ketelslegers, H.B., van Herwijnen, M.H.M., Kleinjans, J.C.S., van Delft, J.H.M., 2010. Comparison of HepG2 and HepaRG by whole-genome gene expression analysis for the purpose of chemical hazard identification. Toxicol. Sci. 115 (1), 66–79.
Jin, R., McConnell, R., Catherine, C., Xu, S., Walker, D.I., Stratakis, N., Jones, D.P., Miller, G.W., Peng, C., Conti, D.V., et al., 2020. Perfluoroalkyl substances and severity of nonalcoholic fatty liver in Children: an untargeted metabolomics approach. Environ. Int. 134, 105220.
Kariuki, M.N., Nagato, E.G., Lankadurai, B.P., Simpson, A.J., Simpson, M.J., 2017. Analysis of Sub-Lethal Toxicity of Perfluorooctane Sulfonate (PFOS) to Daphnia magna Using 1H Nuclear Magnetic Resonance-Based Metabolomics. Metabolites 7 (15).
Kim, S.-A., Lee, Y.-M., Choi, J.-Y., Jacobs, D.R., Lee, D.-H., 2018. Evolutionarily adapted hormesis-inducing stressors can be a practical solution to mitigate harmful effects of chronic exposure to low dose chemical mixtures. Environ. Pollut. 233, 725–734.
Laber, S., Strobel, S., Mercader, J.M., Dashti, H., Dos Santos, F.R.C., Kubitz, P., Jackson, M., Ainbinder, A., Honecker, J., Agrawal, S., et al., 2023. Discovering cellular programs of intrinsic and extrinsic drivers of metabolic traits using LipocyteProfiler. Cell Genom. 3 (7), 100346.
Li, C., Jiang, L., Qi, Y., Zhang, D., Liu, X., Han, W., Ma, W., Xu, L., Jin, Y., Luo, J., et al., 2023. Integration of metabolomics and proteomics reveals the underlying hepatotoxic mechanism of perfluorooctane sulfonate (PFOS) and 6:2 chlorinated polyfluoroalkyl ether sulfonic acid (6:2 Cl-PFESA) in primary human hepatocytes. Ecotoxicol. Environ. Saf. 249, 114361.
Li, S., Park, Y., Duraisingham, S., Strobel, F.H., Khan, N., Soltow, Q.A., Jones, D.P., Pulendran, B., 2013. Predicting network activity from high throughput metabolomics. PLoS Comput. Biol. 9 (7), e1003123.
Lind, L., Zethelius, B., Salihovic, S., van Bavel, B., Lind, P.M.J.D., 2014. Circulating levels of perfluoroalkyl substances and prevalent diabetes in the elderly. Diabetologia 57 (3), 473–479.
Louisse, J., Fragki, S., Rijkers, D., Janssen, A., van Dijk, B., Leenders, L., Staats, M., Bokkers, B., Zeilmaker, M., Piersma, A., et al., 2023. Determination of in vitro hepatotoxic potencies of a series of perfluoroalkyl substances (PFASs) based on gene expression changes in HepaRG liver cells. Arch Toxicol. 97 (4), 1113–1131.
Lu, Y., Pang, Z., Xia, J., 2022. Comprehensive investigation of pathway enrichment methods for functional interpretation of LC–MS global metabolomics data. Brief Bioinform 24 (1).
McGlinchey A, Sinioja T, Lamichhane S, Bodin J, Siljander H, Geng D, Carlsson C, Duberg D, Ilonen J, Virtanen SM *et al*: (2019) **Prenatal Exposure To Environmental Chemicals Modulates Serum Phospholipids In Newborn Infants, Increasing Later Risk Of Type 1 Diabetes**. *bioRxiv* (588350):588350.
Mesnage, R., Biserni, M., Balu, S., Frainay, C., Poupin, N., Jourdan, F., Wozniak, E., Xenakis, T., Mein, C.A., Antoniou, M.N., 2018. Integrated transcriptomics and metabolomics reveal signatures of lipid metabolism dysregulation in HepaRG liver cells exposed to PCB 126. Arch Toxicol. 92 (8), 2533–2547.
Pierozan, P., Kosnik, M., Karlsson, O., 2023. High-content analysis shows synergistic effects of low perfluorooctanoic acid (PFOS) and perfluorooctane sulfonic acid (PFOA) mixture concentrations on human breast epithelial cell carcinogenesis. Environ. Int. 172, 107746.
Pluskal, T., Castillo, S., Villar-Briones, A., Oresic, M., 2010. MZmine 2: modular framework for processing, visualizing, and analyzing mass spectrometry-based molecular profile data. BMC Bioinf. 11, 395.
Pramfalk, C., Larsson, L., Härdfeldt, J., Eriksson, M., Parini, P., 2016. Culturing of HepG2 cells with human serum improve their functionality and suitability in studies of lipid metabolism. Biochim. Biophys. Acta 1861 (1), 51–59.
Rogue, A., Lambert, C., Spire, C., Claude, N., Guillouzo, A., 2012. Interindividual variability in gene expression profiles in human hepatocytes and comparison with HepaRG cells. Drug Metab. Dispos 40 (1), 151–158.
Rose, S., Cuvellier, M., Ezan, F., Carteret, J., Bruyère, A., Legagneux, V., Nesslany, F., Baffet, G., Langouët, S., 2022. DMSO-free highly differentiated HepaRG spheroids for chronic toxicity, liver functions and genotoxicity studies. Arch Toxicol. 96 (1), 243–258.
Rossnerova, A., Izzotti, A., Pulliero, A., Bast, A., Rattan, S.I.S., Rossner, P., 2020. The molecular mechanisms of adaptive response related to environmental stress. Int. J. Mol. Sci. 21 (19), 7053.
Seal, S., Carreras-Puigvert, J., Trapotsi, M.A., Yang, H., Spjuth, O., Bender, A., 2022. Integrating cell morphology with gene expression and chemical structure to aid mitochondrial toxicity detection. Commun Biol. 5 (1), 858.
Seal, S., Carreras-Puigvert, J., Singh, S., Carpenter, A.E., Spjuth, O., Bender, A., 2024. From pixels to phenotypes: integrating image-based profiling with cell health data improves interpretability. Mol. Biol. Cell (mbcE23080298).
Sen, P., Qadri, S., Luukkonen, P.K., Ragnarsdottir, O., McGlinchey, A., Jäntti, S., Juuti, A., Arola, J., Schlezinger, J.J., Webster, T.F., et al., 2022. Exposure to environmental contaminants is associated with altered hepatic lipid metabolism in non-alcoholic fatty liver disease. J. Hepatol 76 (2), 283–293.
Severin, Y., Hale, B.D., Mena, J., Goslings, D., Frey, B.M., Snijder, B., 2022. Multiplexed high-throughput immune cell imaging reveals molecular health-associated phenotypes. Sci. Adv. 8 (44), eabn5631.
Sheng, W., Ji, G., Zhang, L., 2022. The effect of lithocholic acid on the gut-liver axis. Front Pharmacol. 13.
Shiffka, S.J., Jones, J.W., Li, L., Farese, A.M., MacVittie, T.J., Wang, H., Swaan, P.W., Kane, M.A., 2020. Quantification of common and planar bile acids in tissues and cultured cells. J. Lipid Res. 61 (11), 1524–1535.
Sinioja, T., Bodin, J., Duberg, D., Dirven, H., Berntsen, H.F., Zimmer, K., Nygaard, U.C., Oresic, M., Hyotylainen, T., 2022. Exposure to persistent organic pollutants alters the serum metabolome in non-obese diabetic mice. Metabolomics 18 (11), 87.
Sinisalu, L., Yeung, L.W.Y., Wang, J., Pan, Y., Dai, J., Hyötyläinen, T., 2021. Prenatal exposure to poly-/per-fluoroalkyl substances is associated with alteration of lipid profiles in cord-blood. Metabolomics 17 (12), 103.
Stirling, D.R., Swain-Bowden, M.J., Lucas, A.M., Carpenter, A.E., Cimini, B.A., Goodman, A., 2021. Cell Profiler 4: improvements in speed, utility and usability. BMC Bioinf. 22 (1), 433.
Sumner, L.W., Amberg, A., Barrett, D., Beale, M.H., Beger, R., Daykin, C.A., Fan, T.W., Fiehn, O., Goodacre, R., Griffin, J.L., et al., 2007. Proposed minimum reporting standards for chemical analysis Chemical Analysis Working Group (CAWG) Metabolomics Standards Initiative (MSI). Metabolomics 3 (3), 211–221.
Sun, Q., Zong, G., Valvi, D., Nielsen, F., Coull, B., Grandjean, P., 2018. Plasma concentrations of perfluoroalkyl substances and risk of type 2 diabetes: a prospective investigation among U.S Women. Environ. Health Perspectives 126 (3), 037001.
Wang, P., Liu, D., Yan, S., Cui, J., Liang, Y., Ren, S., 2022. Adverse effects of perfluorooctane sulfonate on the liver and relevant mechanisms. Toxics 10 (5).
Xiaopeng, C., Jin, T., 2023. Perfluorooctane sulfonate (PFOS) causes aging damage in the liver through the mt-DNA-mediated NLRP3 signaling pathway. Ecotoxicol Environ. Saf. 262, 115121.
Yang, W., Ling, X., He, S., Cui, H., Yang, Z., An, H., Wang, L., Zou, P., Chen, Q., Liu, J., et al., 2023. PPARα/ACOX1 as a novel target for hepatic lipid metabolism disorders induced by per- and polyfluoroalkyl substances: an integrated approach. Environ. Int. 178, 108138.
Zhang, Y., Zhang, Y., Klaassen, C.D., Cheng, X., 2018. Alteration of bile acid and cholesterol biosynthesis and transport by perfluorononanoic acid (PFNA) in mice. Toxicological Sci: An Official J. Society of Toxicology 162 (1), 225–233.
Zhao, M., Jung, Y., Jiang, Z., Svensson, K.J., 2020. Regulation of energy metabolism by receptor tyrosine kinase ligands. Front Physiol. 11, 354.